CSIRO PUBLISHING

COLLECTION | RESEARCH ARTICLE
https://doi.org/10.1071/ES25027

JOURNAL OF SOUTHERN HEMISPHERE EARTH SYSTEMS SCIENCE

Historical performance and future climate projections from CMIP6 models in central-eastern Argentina

Gabriela V. Müller[A,B,*], María Sol Wilhelm[B], M. Josefina Pierrestegui[A,B] and Miguel A. Lovino[A,B]

For full list of author affiliations and declarations see end of paper

***Correspondence to:**
Gabriela V. Müller
CEVARCAM, FICH, UNL, Ciudad Universitaria, Santa Fe, Argentina
Email: gvmuller@fich.unl.edu.ar

Handling Editor:
Peter May

Received: 3 May 2025
Accepted: 2 October 2025
Published: 19 November 2025

Cite this: Müller GV *et al.* (2025) Historical performance and future climate projections from CMIP6 models in central-eastern Argentina. *Journal of Southern Hemisphere Earth Systems Science* **75**, ES25027. doi:10.1071/ES25027

ABSTRACT

This paper analyses historical climate conditions and future climate projections in central-eastern Argentina, focusing on temperature and precipitation patterns. The study assesses the ability of Coupled Model Intercomparison Project Phase 6 (CMIP6) global climate models to represent historical climate variability and generates projections of precipitation and temperature under three combined socioeconomic and greenhouse gas emissions scenarios for the 21st Century. Historical analysis for the 1901–2014 period reveals high correlations between model-simulated and observed temperature. Precipitation simulations are less accurate; however, bias correction introduces notable improvements. Although the models properly recognise mean annual temperature and precipitation cycles, biases appear in the reproduction of the spatial patterns of these variables. Future projections indicate a significant increase in mean annual temperature across all scenarios, with the highest temperature rise in a fossil-fuel-intensive scenario, highlighting the importance of emissions mitigation. Precipitation is projected to increase in all scenarios, particularly in the western part of the study region, with potential implications for hydrology and agriculture. This study emphasises the need for ongoing research and monitoring to enhance our understanding of regional climate vulnerability and to inform local adaptation strategies in the face of a changing climate.

Keywords: central-eastern Argentina, CMIP6, future projections, model evaluation, precipitation variability, temperature trends.

1. Introduction

The rise in the recorded global average temperature represents one of the most profound transformations in recent times. The prevailing consensus points to human activities as the driving force behind the ~1°C increase in global temperatures above pre-industrial levels (Allen *et al.* 2018*a*; Masson-Delmotte *et al.* 2021). Projections indicate that if current trends persist, the 1.5°C threshold will be crossed sometime between 2030 and 2050 (Allen *et al.* 2018*a*). This trajectory sets the stage for increased occurrence of warm extremes, intense rainfall, prolonged droughts and precipitation deficits in various regions around the globe (Allen *et al.* 2018*b*; Zhang *et al.* 2023).

South-eastern South America (SESA), which encompasses the northern regions of Argentina, Uruguay, southern Brazil and Paraguay, has seen a discernible shift in temperature and precipitation patterns (Junquas *et al.* 2012; Lovino *et al.* 2021; Müller *et al.* 2021; Bigolin and Talamini 2024). These shifts encompass changes in climate variability and the frequency of extreme weather events, which have had a substantial impact on the region (Barros *et al.* 2014; Hagen *et al.* 2022). Temperature extremes in SESA are trending towards warmer conditions (Skansi *et al.* 2013; Carril *et al.* 2016; Lovino *et al.* 2018*a*). This shift manifests in an increased frequency of warm days, warm nights and extended heatwaves, along with a decrease in cold days, cold nights and the duration of cold spells (Lovino *et al.* 2018*a*; Feron *et al.* 2019; Almazroui *et al.* 2021). Annual

Collection: Model evaluation for CMIP and IPCC AR7

precipitation in SESA increased between the 1960s and the 2000s (Barros *et al.* 2008; Seager *et al.* 2010; Lovino *et al.* 2018*b*; Grimm 2019). Extreme precipitation events have also been increasing, resulting in more frequent flash floods (Cavalcanti *et al.* 2015; Avila-Diaz *et al.* 2023; Brêda *et al.* 2023). Additionally, high interannual precipitation variability has contributed to severe droughts, which negatively affect agricultural and livestock productivity (Zambrano *et al.* 2018; Oñate-Valdivieso *et al.* 2020).

The CMIP6 (Coupled Model Intercomparison Project Phase 6) is a comprehensive initiative providing climate model simulations for the 21st Century and beyond (Eyring *et al.* 2016, 2019; O'Neill *et al.* 2016). These simulations serve as a basis for projecting future climate changes, including changes in temperature and precipitation patterns (Almazroui *et al.* 2020; Lovino *et al.* 2021; Tebaldi *et al.* 2021; Zareian *et al.* 2024). Several studies have assessed the performance of CMIP6 models in predicting temperature and precipitation changes across different regions worldwide (e.g. Kim *et al.* 2020; Carvalho *et al.* 2021; Tian *et al.* 2021). For instance, Zareian *et al.* (2024) analysed precipitation estimates from historical runs of CMIP6 models across various climatic zones. They found that the models generally perform well in capturing broad spatial patterns of precipitation but exhibit significant biases in regions with complex topography and in arid and semi-arid zones. Specifically, overestimations were noted in tropical and monsoon regions, whereas underestimations were prevalent in subtropical dry areas. These discrepancies highlight the need for regional downscaling and bias correction methods to improve the applicability of CMIP6 outputs in local climate impact studies. Additionally, inter-model variability underscores the importance of using ensemble approaches to better quantify uncertainties and improve the robustness of climate projections in diverse climatic zones. Almazroui *et al.* (2021) evaluated CMIP6 models' ability to project temperature and precipitation changes in South America, reporting that the models generally capture the observed temperature trends across the continent. However, precipitation projections showed higher uncertainty, particularly in regions influenced by complex climatic drivers such as the Amazon basin and the Andes. The study highlighted substantial inter-model variability in simulating seasonal precipitation patterns, emphasising the need for improved model parameterisation and the integration of localised data to enhance prediction accuracy in these critical areas. Overall, CMIP6 models have exhibited commendable accuracy in replicating the spatial distribution of temperature and precipitation patterns. Nevertheless, further research is needed to better know the biases and uncertainties still present in the models.

The potential for climate-related disasters, stemming from anthropogenic climate change and natural climate variability, can result in shifts in exposure and vulnerability for both human and natural systems (Formetta and Feyen 2019). Climate change also poses a risk to biodiversity and increases the likelihood of extreme weather events (e.g. Muluneh 2021; Hagen *et al.* 2022). Climate projections for SESA by 2100 under medium to high emissions scenarios (representative concentration pathways or RCPs) suggest a warming range of 1.7–6.7°C, accompanied by an increase in the number of warm days and nights, as well as a 25% rise in precipitation (Masson-Delmotte *et al.* 2021). This study assesses the ability of CMIP6 model simulations to represent the historical and current climate conditions in central-eastern Argentina and analyses temperature and precipitation projections under three socioeconomic development and greenhouse gas (GHG) emissions scenarios in the short-term (2021–2040), mid-term (2041–2060) and long-term (2081–2100). Section 2 presents the data and methods used. Section 3 exhibits the historical analysis, and Section 4 discusses the future projections. Section 5 presents the concluding remarks.

2. Data and methods

2.1. Study region

This study concentrates on an extended plain region with minimal slopes, known as the core crop region (CCR, Sgroi *et al.* 2021) in central-eastern Argentina. The CCR comprises 58–65°W and 26–36°S (Fig. 1) and is the country's primary agricultural area, accounting for over 80% of Argentina's

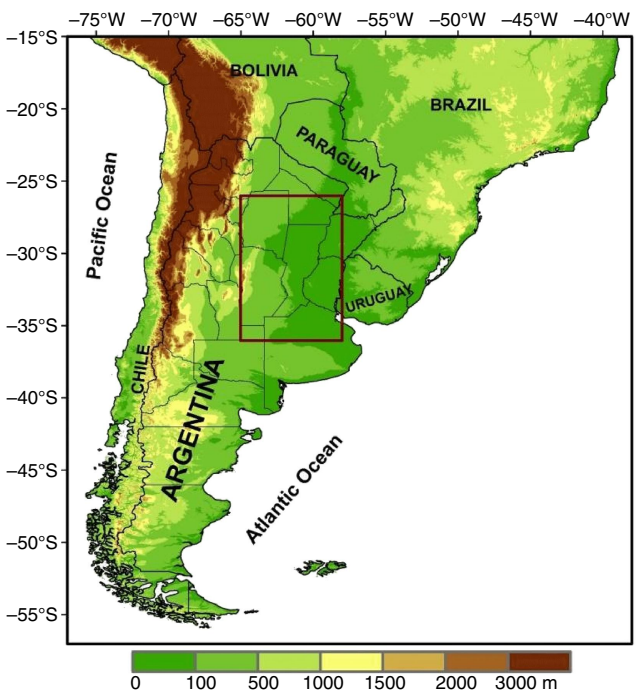

Fig. 1. Topography map of southern South America. The study region encompassing the core crop region in central-eastern Argentina is highlighted with a red rectangle.

total crop production (Ministerio de Agricultura, Ganadería y Pesca de Argentina 2021). Owing to its agricultural output, Argentina plays a key role in global food security, exporting large quantities of grains and livestock products, including corn, soybean, barley, rice, flaxseed and beef (World Bank 2024).

According to the Köppen–Trewartha climate classification, the CCR has a humid subtropical climate (Jacob *et al.* 2012; Gallardo *et al.* 2016). Precipitation is evenly distributed throughout the year, and the thermal gradient follows a latitudinal pattern (Garreaud *et al.* 2009). The CCR has high hydro-climatic variability from interannual to decadal timescales. In recent decades, the frequency and intensity of extreme weather events have increased (Barros *et al.* 2014; Castellanos *et al.* 2022). Given its economic significance and the concentration of agricultural and industrial activities, the CCR is home to a large portion of Argentina's population. As a result, the region is particularly vulnerable to hydroclimatic variability and extreme events, which pose risks to both food production and socioeconomic stability.

2.2. Data

This study utilises a set of multi-member simulations from 22 global climate models (GCMs) of the CMIP6, developed by various modelling centres (Table 1). The 22 selected models were chosen based on data availability across all scenarios, the diversity of modelling centres and the inclusion of models with multiple ensemble members to enhance ensemble robustness. The CMIP6 archive provides historical climate simulations for 1850–2014 (Eyring *et al.* 2016). This study evaluates historical simulations of monthly precipitation and surface air temperature over the 1901–2014 period. For each GCM, multi-member ensembles were generated from multiple realisations that differ only in their initial conditions (see Table 1). These single-model ensembles were subsequently combined to form a multi-model ensemble. Such ensemble construction methodology effectively reduces both the internal variability of the climate system and model uncertainties, which enhances the detection of observed climate signals and provides more reliable projections (Deser 2020; Lehner *et al.* 2020).

The CMIP6 also includes future scenario simulations based on different socioeconomic trajectories known as the Shared Socioeconomic Pathways (SSPs, Riahi *et al.* 2017). These scenarios represent plausible evolutions of societal, economic, technological and environmental factors (O'Neill 2016). The SSPs are structured into five distinct narratives: sustainable development (SSP1), middle-of-the-road development (SSP2), regional rivalry (SSP3), inequality (SSP4) and fossil-fuelled development (SSP5) (O'Neill *et al.* 2016). These socioeconomic pathways are combined with different GHG emission trajectories based on four Representative Concentration Pathways (RCPs), characterised by radiative forcing levels of 2.6, 4.5, 6.0 and 8.5 W m^{-2} by the year 2100. The integration of climate model projections with these socioeconomic pathways results in combined scenarios referred to as SSP*x*–*y*, where '*x*' denotes the specific socioeconomic pathway and '*y*' represents the corresponding radiative forcing level (O'Neill *et al.* 2016). This study focuses on three of these integrated scenarios: SSP1–2.6, SSP2–4.5 and SSP5–8.5. We follow the IPCC's core scenario set by including SSP5–8.5, which, despite being increasingly considered unlikely, still represents a plausible very-high emissions future that cannot be ruled out given uncertainties in feedbacks and socioeconomic trajectories. The performance of the GCMs was assessed by comparing their simulations against gridded observational datasets of monthly temperature and precipitation from CRU TS 4.05 (Harris *et al.* 2020), which provide data at a 0.5 × 0.5° spatial resolution for the period 1901–2020.

2.3. Evaluation methodology

A series of preprocessing steps were applied to the GCM outputs. First, all simulations were interpolated to a common 1 × 1° grid using bilinear interpolation, following methodologies from previous studies (e.g. Zazulie *et al.* 2017). Next, model performance was assessed by comparing the mean annual cycles and spatial patterns of temperature and precipitation against observations for the period 1985–2014, which represents the most recent normal period available within the study period of 1901–2014. Annual cycles and spatial patterns were also constructed for the 1931–1961 period, to assess how the models reproduce the regional changes in temperature and precipitation.

To quantify model performance, several statistical metrics were computed, including the mean bias error (MBE), mean absolute error (MAE), root mean square error (RMSE), Nash–Sutcliffe efficiency (NSE) and Pearson correlation coefficient (*r*). Definitions and further details on these metrics are provided in Déqué (2012), Nash and Sutcliffe (1970) and Moriasi *et al.* (2007). Whereas MBE indicates whether the model systematically overestimates or underestimates observed values, MAE and RMSE provide insight into the magnitude of errors. A NSE value of 1 indicates perfect agreement between simulated and observed data, whereas a NSE of 0 suggests that the model's RMSE is equivalent to the variance of the observed data. Negative NSE values indicate that the RMSE exceeds the variance of the observed data.

To correct systematic biases in GCM outputs and improve their alignment with historical observations, a scaling method based on Maraun *et al.* (2010) was applied. This method involves computing a scaling factor (Eqn 1), defined as the ratio between the mean observed value and the mean simulated value over the historical reference period. The corrected variable at a given time step is then obtained by multiplying the modelled value by this factor. Specifically, the corrected variable, denoted as y_i^{p}, at time i is represented as the modelled variable $x_{\mathrm{mod},i}^{\mathrm{p}}$, scaled with the

Table 1. CMIP6 models used and their attributes.

	Model	Institution, country	Experiments (number of members)	Resolution (° lat × ° long)
1	ACCESS-CM2	CSIRO-ARCCSS, Australia	Historical (3), SSP1–2.6 (3), SSP2–4.5 (3), SSP5–8.5 (3)	1.25 × 1.875
2	ACCESS-ESM1-5	CSIRO, Australia	Historical (10), SSP1–2.6 (3), SSP2–4.5 (3), SSP5–8.5 (3)	1.25 × 1.875
3	BCC-CSM2-MR	BCC, China	Historical (3), SSP1–2.6 (1), SSP2–4.5 (1), SSP5–8.5 (1)	1.125 × 1.125
4	CAMS-CSM1-0	CAMS, PR China	Historical (3), SSP1–2.6 (2), SSP2–4.5 (2), SSP5–8.5 (2)	1.125 × .125
5	CanESM5	CCCma, Canada	Historical (10), SSP1–2.6 (10), SSP2–4.5 (10), SSP5–8.5 (10),	2.8 × 2.8
6	CESM2	NCAR, USA	Historical (6), SSP1–2.6 (5), SSP2–4.5 (4), SSP5–8.5 (5)	0.9375 × 1.25
7	CESM2-WACCM	NCAR, USA	Historical (3), SSP1–2.6 (1), SSP2–4.5 (5), SSP5–8.5 (5)	0.9375 × 1.25
8	EC-Earth3	EC-Earth-Consortium, Sweden	Historical (6), SSP1–2.6 (6), SSP2–4.5 (6), SSP5–8.5 (6)	0.93 × 0.93
9	FGOALS-f3-L	CAS, PR China	Historical (3), SSP1–2.6 (1), SSP2–4.5 (1), SSP5–8.5 (1)	1.25 × 1
10	FGOALS-g3	CAS, PR China	Historical (6), SSP1–2.6 (1), SSP2–4.5 (4), SSP5–8.5 (4)	2 × 2.25
11	FIO-ESM2-0	FIO-QLNM, PR China	Historical (3), SSP1–2.6 (3), SSP2–4.5 (3), SSP5–8.5 (3)	0.9375 × 1.25
12	GISS-E2-1-H	NASA Goddard Institute for Space Studies, USA	Historical (3), SSP1–2.6 (3), SSP2–4.5 (3), SSP5–8.5 (3)	2.0 × 2.5
13	HadGEM3-GC31-LL	MOHC, UK	Historical (4), SSP1–2.6 (1), SSP2–4.5 (1), SSP5–8.5 (4)	1.25 × 1.875
14	HadGEM3-GC31-MM	MOHC, UK	Historical (4), SSP1–2.6 (1), SSP5–8.5 (3)	0.5 × 0.83
15	INM-CM5-0	INM, Russian Federation	Historical (10), SSP1–2.6 (1), SSP2–4.5 (1), SSP5–8.5 (1)	1.5 × 2
16	IPSL-CM6A-LR	IPSL, France	Historical (10), SSP1–2.6 (6), SSP2–4.5 (10), SSP5–8.5 (6)	1.25 × 2.5
17	KACE-1-0-G	NIMS-KMA, South Korea	Historical (3), SSP1–2.6 (3), SSP2–4.5 (3), SSP5–8.5 (3)	1.25 × 1.875
18	MIROC6	MIROC, Japan	Historical (10), SSP1–2.6 (10), SSP2–4.5 (3), SSP5–8.5 (10)	1.41 × 1.41
19	MPI-ESM1-2-HR	MPI-M, Germany	Historical (10), SSP1–2.6 (2), SSP2–4.5 (2), SSP5–8.5 (2)	0.937 × 0.937
20	MPI-ESM1-2-LR	MPI-M, Germany	Historical (10), SSP1–2.6 (10), SSP2–4.5 (10), SSP5–8.5 (10)	1.875 × 1.875
21	MRI-ESM2.0	MRI, Japan	Historical (6), SSP1–2.6 (1), SSP2–4.5 (1), SSP5–8.5 (2)	1.125 × 1.125
22	NorESM2-MM	NCC, Norway	Historical (3), SSP1–2.6 (1), SSP2–4.5 (1), SSP5–8.5 (1)	0.9375 × 1.25

Experiments include both historical simulations and future projections within integrated scenarios denoted as SSP*x*–*y*. Here '*x*' indicates the particular Shared Socioeconomic Pathway (SSP), whereas '*y*' denotes the forcing pathway determined by its long-term global average radiative forcing level.

ratio of the mean observed variable $\underline{y}^{\mathrm{p}}_{\mathrm{obs}}$, and the mean modelled variable $\underline{y}^{\mathrm{p}}_{\mathrm{mod}}$.

$$y_i^{\mathrm{p}} = x^{\mathrm{p}}_{\mathrm{mod},i} \times \frac{\underline{y}^{\mathrm{p}}_{\mathrm{obs}}}{\underline{y}^{\mathrm{p}}_{\mathrm{mod}}} \quad (1)$$

The scaling method was applied to both historical and future simulations. Historical simulations were corrected using the CRU TS 4.05 data as a $\underline{y}^{\mathrm{p}}_{\mathrm{obs}}$, such that the MBE of the bias-corrected time series becomes zero. Future simulations were corrected using the scaling factor used for historical simulations:

$$y_i^{\mathrm{f}} = x^{\mathrm{f}}_{\mathrm{mod},i} \times \frac{\underline{y}^{\mathrm{p}}_{\mathrm{obs}}}{\underline{y}^{\mathrm{p}}_{\mathrm{mod}}} \quad (2)$$

where f indicates future and p means past. The purpose of this bias correction is twofold: (a) to adjust systematic errors in historical simulations and (b) to align the trajectory of future projections with observed historical values while preserving model-projected changes.

2.4. Projected scenarios

Future projections of temperature and precipitation were generated and analysed for three distinct time horizons – near-term (2021–2040), mid-term (2041–2060) and long-term (2081–2100) – following the standard periods used in IPCC AR6 to ensure consistency with global assessments (Lee *et al.* 2021). The assessment includes three integrated SSP scenarios: SSP1–2.6, which represents a sustainable development pathway with strong mitigation efforts; SSP2–4.5, reflecting moderate socioeconomic development and stabilisation of GHG emissions; and SSP5–8.5, corresponding to high fossil-fuel dependency and elevated GHG emissions. We analysed area-averaged time series from bias-corrected multi-model ensembles. Additionally, we determined the mean spatial changes for each period and scenario using non-corrected multi-model ensembles of historical and future simulations, ensuring that estimates remain unaffected by bias-correction methods. Average changes were calculated by comparing simulations from the 'near present' period (1995–2014) with future short-, mid- and long-term periods.

3. Results

3.1. Historical analysis

3.1.1. Temperature

Table 2 presents the model evaluation metrics, indicating that all simulations capture the observed temperature with high correlations (0.95–0.97) and relatively low error magnitudes (MBE, 0.11–5.71; MAE, 1.20–5.71; RMSE, 1.51–6.00). The application of the scaling method leads to a substantial reduction in MAE and RMSE (MAE*, 1.02–2.10; RMSE*, 1.29–2.51) and enhances NSE, particularly for models exhibiting systematic biases. Notably, simulations with pronounced MBEs (e.g. models in rows 12, 18, 20 and 22) show the most significant improvements after scaling. By contrast, models with non-systematic errors experience minimal changes, as the method effectively rectifies mean values but preserves key statistical properties of the time series, such as standard deviation (e.g. models in rows 5, 15 and 16). When evaluating the multi-model ensemble, the combined 22-model ensemble achieves the best overall performance, yielding a correlation coefficient of 0.97, a reduced RMSE of 1.36°C and a NSE* of 0.92, underscoring the robustness of ensemble-based approaches in minimising individual model uncertainties.

We analysed the mean temperature annual cycle (Fig. 2) for the historical periods 1931–1960 and 1985–2014 to assess potential changes over time. The 22-model ensemble effectively captures the observed seasonal patterns but exhibits a systematic warm bias during the warmer months (September–April; Fig. 2*a*, *b*). After applying bias correction to mitigate systematic errors (Fig. 2*c*, *d*), the inter-model range is significantly reduced from an average of 6.97–2.81°C. Although this adjustment decreases the overestimation in the warm season, a slight positive bias persists during the colder months (May–August). Overall, no substantial differences are detected between the mean annual cycles of the two analysed periods. In both cases, the multi-model ensemble demonstrates a strong agreement with observed temperature patterns, reinforcing its reliability in simulating historical climate variability.

Fig. 3 reveals that the observed temperature gradient, characterised by a gradual decrease from north to south (Fig. 3*a*), is reasonably well captured by the 22-model ensemble (Fig. 3*b*). However, the ensemble exhibits a slight warm bias, particularly near the low mountain ranges in the south-western corner of the study region (Fig. 3*c*). Across most of the region, temperature overestimations are ~1°C, but reach 4°C at higher elevations. Conversely, a slight cold bias is observed in the north-western corner, where elevations approach 1000 m ASL.

3.1.2. Precipitation

Table 3 presents the statistical metrics used to assess the performance of the GCMs in simulating the historical precipitation regime over the region. Correlation coefficients for individual models range within 0.40–0.74. The multi-model ensemble achieves the highest correlation (r = 0.76), reinforcing the benefits of ensemble averaging in reducing model uncertainties. Other statistical metrics, such as MAE and RMSE, fall within acceptable ranges (7.38 < MBE < 21.17; 21.64 < MAE < 38.36; 28.97 < RMSE < 48.28) when compared to previous studies (e.g. Lovino *et al.* 2018*a*, 2021). After bias correction, a significant reduction in

Table 2. Statistical evaluation metrics (simulations *v.* observations) of area-averaged mean temperature for the historical period 1901–2014.

	Model	MBE (°C month^{-1})	MAE (°C month^{-1})	RMSE (°C month^{-1})	NSE	Correlation coefficient	MAE* (°C month^{-1})	RMSE* (°C month^{-1})	NSE*
1	ACCESS-CM2	0.11	1.42	1.78	0.86	0.96	1.39	1.76	0.87
2	ACCESS-ESM1-5	0.98	1.70	2.03	0.82	0.97	1.26	1.58	0.89
3	BCC-CSM2-MR	1.02	1.87	2.27	0.78	0.96	1.44	1.80	0.86
4	CAMS-CSM1-0	0.49	2.28	2.71	0.68	0.96	2.10	2.51	0.72
5	CanESM5	-1.38	1.53	1.93	0.84	0.97	1.24	1.56	0.89
6	CESM2	2.14	2.32	2.63	0.70	0.96	1.05	1.33	0.92
7	CESM2-WACCM	2.19	2.38	2.72	0.68	0.96	1.09	1.40	0.91
8	EC-Earth3	1.05	1.56	1.92	0.84	0.95	1.21	1.51	0.90
9	FGOALS-f3-L	1.04	1.53	1.86	0.85	0.96	1.11	1.43	0.91
10	FGOALS-g3	1.03	1.64	1.93	0.84	0.96	1.15	1.47	0.91
11	FIO-ESM2-2-0	1.08	1.49	1.80	0.86	0.96	1.11	1.41	0.91
12	GISS-E2-1-H	3.70	3.77	4.26	0.21	0.97	1.12	1.41	0.91
13	HadGEM-GC31-LL	0.78	1.48	1.80	0.86	0.96	1.19	1.50	0.90
14	HadGEM-GC31-MM	0.13	1.20	1.51	0.90	0.96	1.18	1.49	0.90
15	INM-CM5-0	-0.52	1.69	2.06	0.82	0.97	1.79	2.13	0.80
16	IPSL-CM6A-LR	0.57	1.42	1.71	0.87	0.96	1.22	1.52	0.90
17	KACE-1-0-G	1.54	2.09	2.51	0.73	0.96	1.33	1.66	0.88
18	MIROC6	5.71	5.71	6.00	-0.57	0.96	1.02	1.29	0.93
19	MPI-ESM1-2-HR	0.47	1.26	1.57	0.89	0.96	1.15	1.44	0.91
20	MPI-ESM1-2-LR	2.39	2.59	3.09	0.58	0.96	1.22	1.53	0.90
21	MRI-ESM2.0	1.26	1.76	2.12	0.80	0.96	1.18	1.48	0.90
22	NorESM2-MM	3.00	3.08	3.44	0.48	0.96	1.05	1.34	0.92
23	Ensemble	1.23	1.68	1.98	0.83	0.97	1.08	1.36	0.92

MBE, mean bias error (°C month^{-1}); MAE, mean absolute error (°C month^{-1}); RMSE, root mean square error (°C month^{-1}); NSE, Nash–Sutcliffe efficiency; *r*, Pearson correlation coefficient. Evaluation metrics for the bias-corrected time series are MAE*, RMSE* and NSE*.

errors is observed ($21.46 < \text{MAE}^* < 30.48$; $27.83 < \text{RMSE}^* < 39.41$), indicating that the correction method effectively mitigates biases and enhances the models' ability to reproduce historical precipitation patterns.

Fig. 4 compares the observed and simulated annual precipitation cycles before and after bias correction for the periods 1931–1960 and 1985–2014. The model ensemble successfully captures the observed annual cycle in both periods but systematically underestimates precipitation for January–April. The largest discrepancy occurs in March, coinciding with a maximum local precipitation. The inter-model range is higher during the rainy season of November–April than in the drier winter months (June–August). During the rainy season, the inter-model range amplitude is almost 100 mm, whereas during June–August, the inter-model range drops to almost 50 mm.

The observed precipitation gradient is characterised by isohyets with north–south orientation, with precipitation decreasing from east to west. The 19-model ensemble captures this spatial pattern but systematically underestimates annual precipitation values across the region. Observed annual precipitation (Fig. 5*a*) range is 500–1600 mm year^{-1}, with maximum precipitation in the north-eastern sector. Although the ensemble reproduces the overall spatial distribution (Fig. 5*b*), it notably underestimates annual precipitation, particularly in the central region, including eastern Córdoba, Santa Fe and Entre Ríos. This systematic bias, with annual underestimations reaching ~250 mm, highlights the challenges of accurately simulating precipitation patterns, which are crucial for hydrological and agricultural applications in the region.

3.2. Projections

To assess future climate changes, we analyse the time series of mean annual temperature and total annual precipitation spanning the historical period (1901–2014) and the projected period (2015–2100). In addition, the spatial distribution of projected changes in annual precipitation and mean

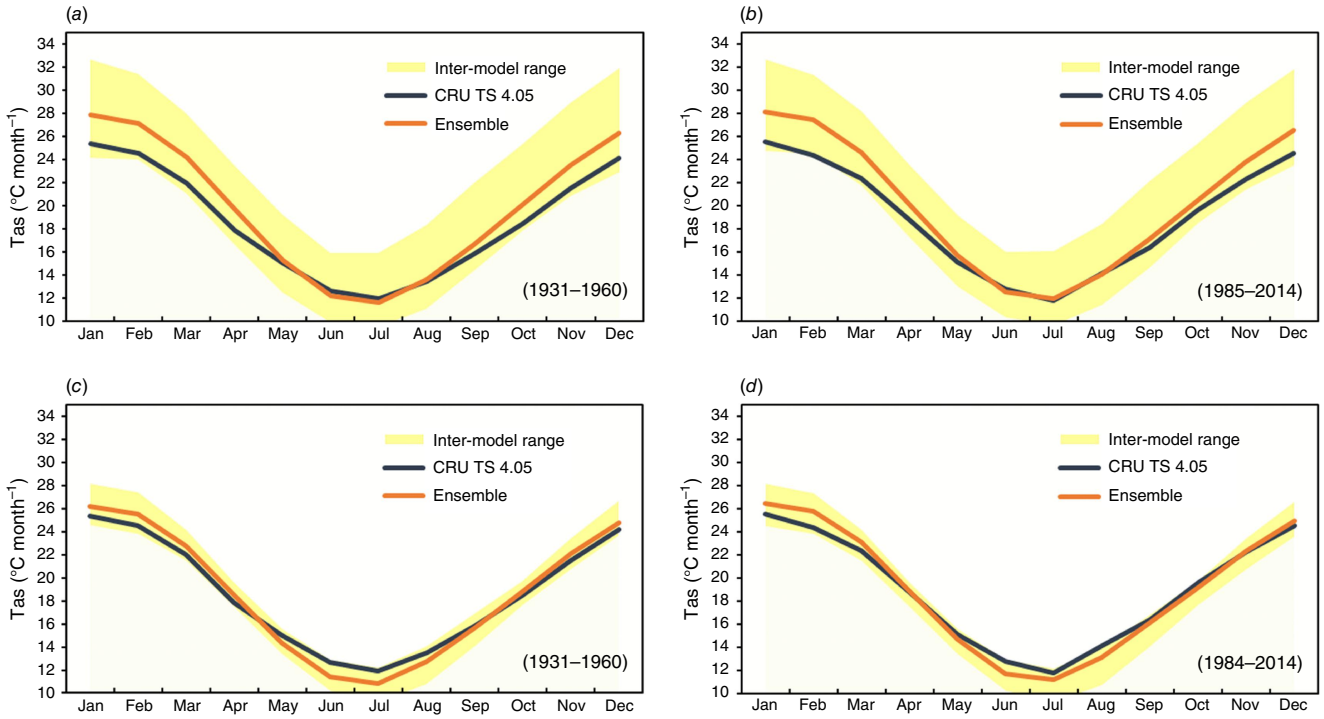

Fig. 2. Comparison of the mean annual cycle of (*a*) observed and (*b*) modelled mean temperature by the 22-model ensemble for the historical periods 1931–1960 and 1985–2014 respectively. Shades represent inter-model ranges. Panels (*c*) and (*d*) are respectively like (*a*) and (*b*), but for the bias-corrected 22-model ensemble.

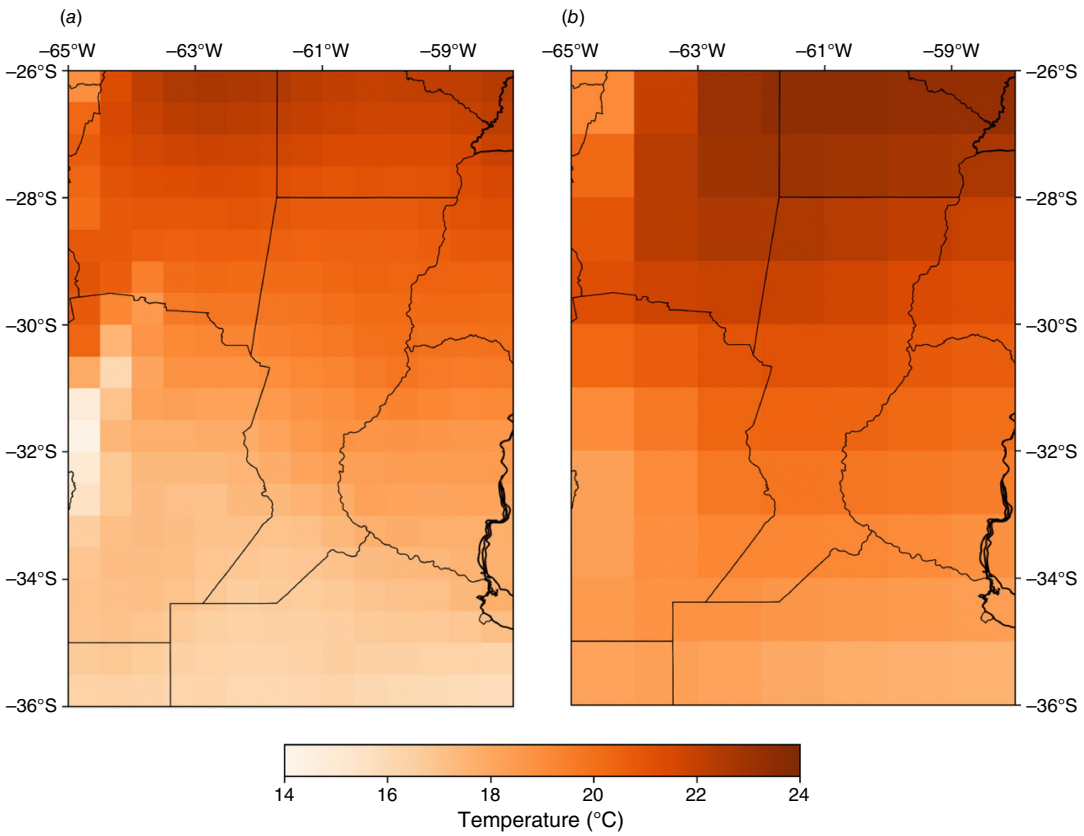

Fig. 3. Spatial distribution (1985–2014 period) of the (*a*) observed mean annual temperature and (*b*) bias-corrected 22-model ensemble.

Table 3. Statistical evaluation metrics (simulations *v*. observations) of area-averaged precipitation over the historical period 1901–2014.

	Model	MBE (mm month^{-1})	MAE (mm month^{-1})	RMSE (mm month^{-1})	NSE	*r*	MAE* (mm month^{-1})	RMSE* (mm month^{-1})	NSE*
1	ACCESS-CM2	15.49	29.81	38.82	0.18	0.65	25.11	33.17	0.40
2	ACCESS-ESM1-5	7.38	24.57	30.75	0.48	0.72	23.32	29.95	0.51
3	BCC-CSM2-MR	-15.79	27.38	36.45	0.28	0.64	25.94	32.94	0.41
4	CanESM5	13.11	29.68	39.72	0.14	0.71	25.44	33.43	0.39
5	CESM2	-11.26	23.54	30.96	0.48	0.74	23.21	30.27	0.50
6	CESM2-WACCM	-14.07	25.69	34.27	0.36	0.69	25.92	33.88	0.38
7	EC-Earth3	21.17	38.36	48.28	-0.27	0.50	30.48	39.41	0.15
8	FGOALS-f3-L	-23.33	30.00	39.29	0.16	0.68	27.70	36.44	0.28
9	FGOALS-g3	-28.08	31.33	40.99	0.09	0.73	24.22	31.75	0.45
10	FIO-ESM2-2-0	1.14	26.29	34.00	0.37	0.71	26.02	33.65	0.38
11	HadGEM-GC31-LL	10.92	27.11	34.82	0.34	0.68	24.42	31.77	0.45
12	INM-CM5-0	-23.37	29.37	38.70	0.18	0.70	27.14	35.73	0.30
13	IPSL-CM6A-LR	-17.01	27.02	34.67	0.35	0.73	27.56	35.25	0.32
14	KACE-1-0-G	-12.24	25.98	34.29	0.36	0.69	26.29	34.76	0.34
15	MIROC6	-23.04	28.21	37.85	0.22	0.72	23.69	30.82	0.48
16	MPI-ESM1-2-HR	7.88	26.01	32.28	0.43	0.68	24.80	31.64	0.45
17	MPI-ESM1-2-LR	-16.26	32.42	42.58	0.01	0.40	31.56	39.31	0.16
18	MRI-ESM2.0	-18.77	29.52	39.39	0.15	0.61	26.33	33.97	0.37
19	NorESM2-MM	-18.54	30.45	40.83	0.09	0.53	29.04	38.34	0.20
	Ensemble	-7.61	21.64	28.97	0.54	0.76	21.46	27.83	0.58

MBE, mean bias error (mm month^{-1}); MAE, mean absolute error (mm month^{-1}); RMSE, root mean square error (mm month^{-1}); NSE, Nash–Sutcliffe efficiency; *r*, Pearson correlation coefficient. Evaluation metrics of the bias-corrected time series are MAE*, RMSE* and NSE*.

annual temperature are examined for three future periods – short-term (2021–2040), medium-term (2041–2060) and long-term (2081–2100) – relative to the historical baseline (1995–2014). The projections reveal an overall increase in both variables, with more pronounced changes under higher GHG emissions and fossil fuel-based development scenarios.

3.2.1. Temperature projections

The projected evolution of mean annual temperature (Fig. 6) indicates a consistent warming trend across all scenarios, with the magnitude of warming depending on the combination of development pathway and GHG emissions scenario. Under the SSP5–8.5 scenario, which combines fossil fuel-driven development with high GHG emissions, the mean annual temperature is projected to increase by 3.5°C by 2100, reaching 22.9°C compared to the 2014 observed average of 19.4°C (Fig. 6*c*). The warming trend is continuous under this scenario, with no indication of stabilisation. In the SSP2–4.5 scenario, mean temperature increases gradually, reaching 1.28°C above the historical average by 2100, with stabilisation occurring toward the end of the century (Fig. 6*b*). Under the SSP1–2.6 scenario, the projected increase is more modest, reaching 0.56°C above historical levels, with a peak *c*. 2060 followed by a slight decline after 2080 (Fig. 6*a*).

The spatial distribution of mean annual temperature change (Fig. 7) reveals a consistent warming pattern across the region, with greater increases in the northern sector. The magnitude of warming intensifies over time and varies across scenarios, with projected temperature changes in the range 0.5–4.5°C by the late 21st Century. The most pronounced warming occurs under the SSP5–8.5 scenario, emphasising the potential consequences of fossil fuel-driven development and high GHG emissions.

3.2.2. Precipitation projections

Future projections suggest a slight increase in total annual precipitation throughout the 21st Century across all combined development and emissions scenarios (Fig. 8). However, these changes are characterised by substantial uncertainty due to the large inter-model spread and the inherent temporal variability of precipitation. By 2100, the projected increase ranges from ~50 mm in the SSP1–2.6

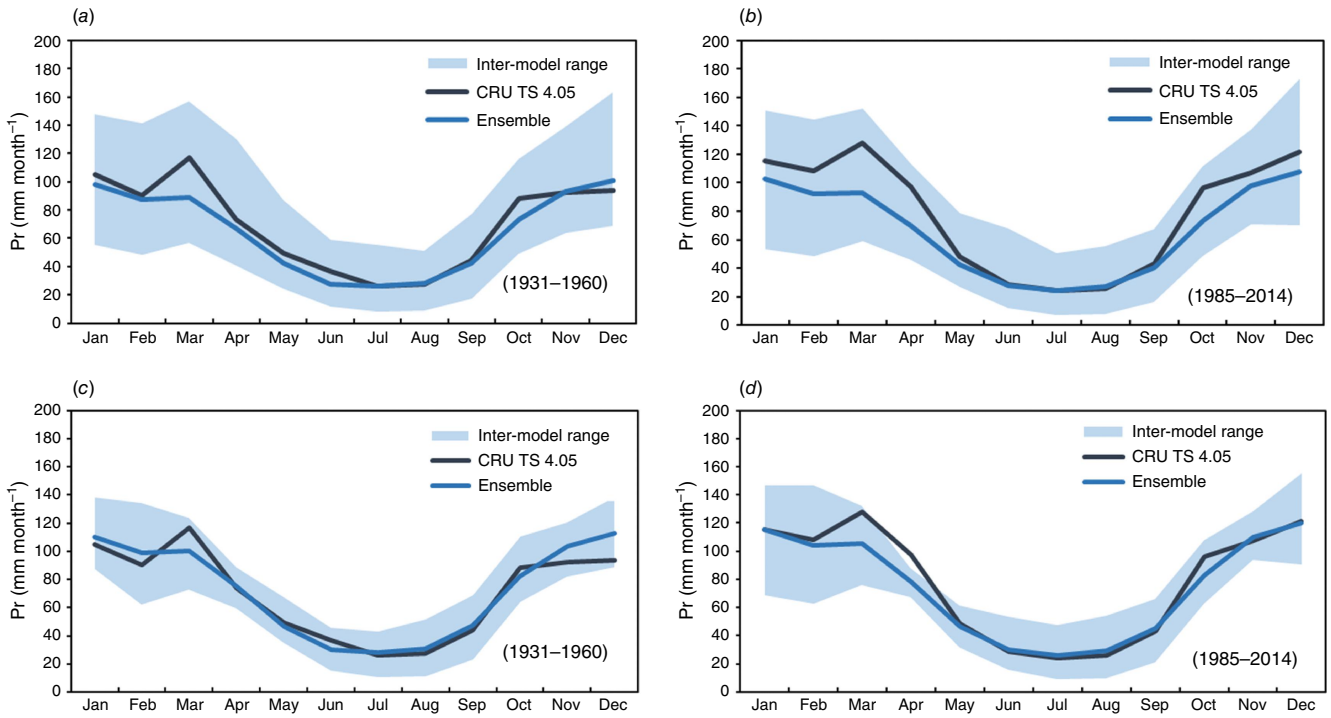

Fig. 4. Comparison of the mean annual cycle of (*a*) observed and (*b*) modelled precipitation by the 19-model ensemble for the historical periods 1931–1960 and 1985–2014 respectively. Shades represent inter-model ranges. Panels (*c*) and (*d*) are respectively like (*a*) and (*b*), but for the bias-corrected 19-model ensemble.

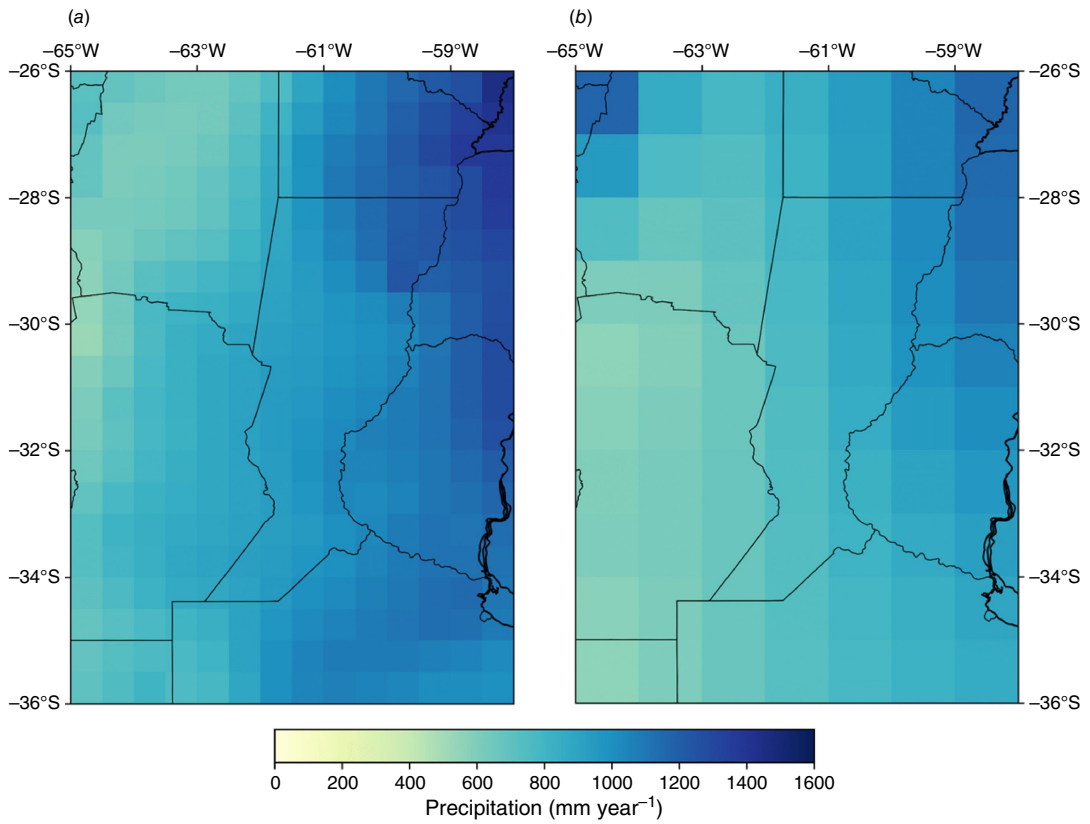

Fig. 5. Spatial distribution (1985–2014 period) of (*a*) the observed annual precipitation and (*b*) the bias-corrected 19-model ensemble.

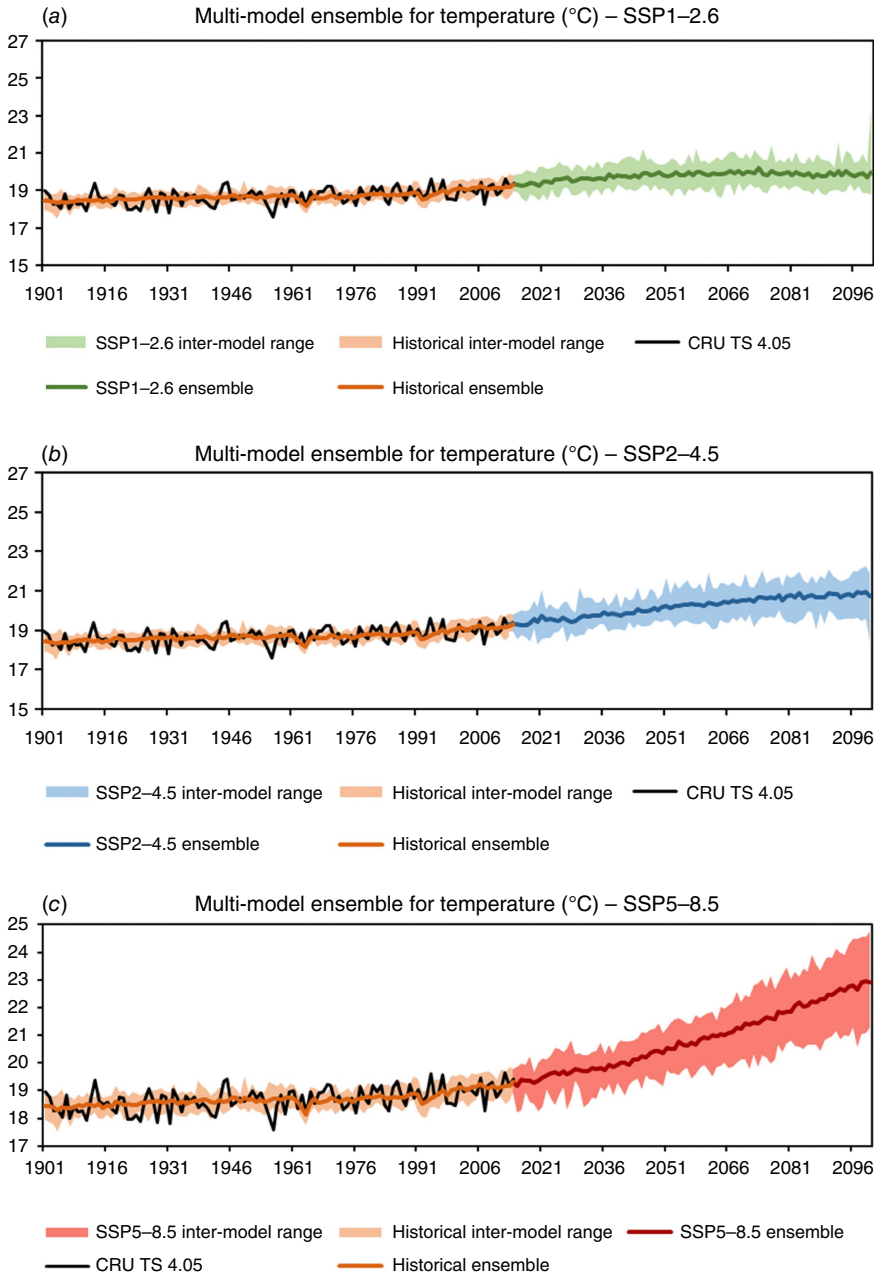

Fig. 6. Observed and bias-corrected model-simulated mean annual temperature for the historical period (1901–2014) and bias-corrected simulated future temperature (2015–2100). Panels (*a*), (*b*) and (c) correspond to scenarios SSP1–2.6, SSP2–4.5 and SSP5–8.5. Historical and future multi-model ensemble simulations were performed using the multi-member mean simulations of 19 analysed GCMs (see Table 1). Shaded areas represent inter-model ranges.

scenario (Fig. 8*a*) to 80 mm in the SSP5–8.5 scenario (Fig. 8*c*), representing an increase of less than 10% relative to the regional mean annual precipitation of ~1000 mm. This modest increase in total precipitation is particularly relevant when considering the high interannual variability of rainfall in the region (Lovino *et al.* 2018*b*), which may overshadow long-term trends.

The temporal evolution of annual precipitation reveals scenario-dependent differences in the rate of change (Fig. 8). In the SSP1–2.6 scenario, precipitation exhibits an initial increase followed by stabilisation towards the late 21st Century (Fig. 8*a*). By contrast, under SSP2–4.5 and SSP5–8.5, precipitation continues to rise over time, with a more pronounced increase in the latter scenario, reflecting the influence of a high-emissions, fossil fuel-driven development pathway (Fig. 8*b*, *c*).

The spatial distribution of projected annual precipitation changes shows greater uniformity across scenarios compared to temperature; however, notable regional variations persist (Fig. 9). Across all scenarios, precipitation increases are more pronounced in the western sector of the study region, with localised increases of ~50 mm year^{-1}. This pattern remains consistent throughout the century. Note that the systematic underestimations in modelled historical precipitation found in this study should be considered when interpreting these projections.

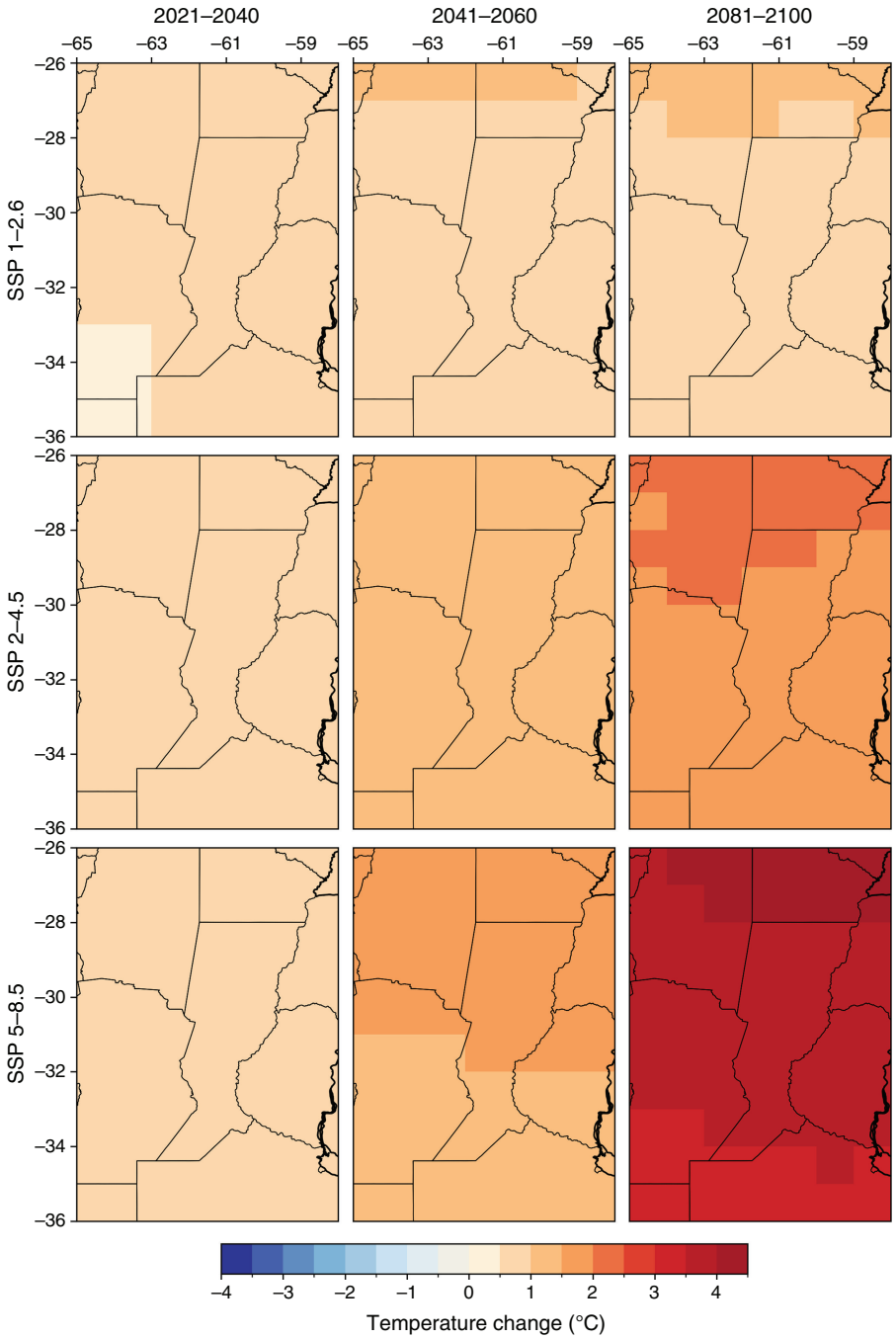

Fig. 7. Spatial distribution of future average changes in mean annual temperature (°C) according to the non-corrected 22-model ensemble over the core crop region in Argentina in the periods (columns) 2021–2040, 2041–2060 and 2081–2100. Average changes are related to the 'near present' 1995–2014 period for the non-corrected 22-model ensemble of historical simulations. Rows correspond to scenarios SSP1–2.6, SSP2–4.5 and SSP5–8.5.

4. Conclusions

This study evaluates historical climate conditions and provides future projections of temperature and precipitation over the CCR in central-eastern Argentina, one of the most productive agricultural areas globally. Given the region's crucial role in food production and export, understanding past climate variability and future trends is essential for anticipating potential impacts on agriculture, water resources and socioeconomic stability. By analysing historical climate simulations and future projections under different socioeconomic development and GHG emission scenarios, this study provides valuable insights into anticipated climatic changes and their implications for regional sustainability and agricultural resilience.

The evaluation of historical climate conditions reveals that global climate models adequately reproduce the annual cycle of mean temperature and its spatial distribution, despite a systematic warm-season overestimation. The application of bias correction significantly reduces these errors, improving the accuracy of modelled temperature values. Precipitation simulations present greater uncertainties, with a systematic underestimation of annual totals, particularly in central areas of the

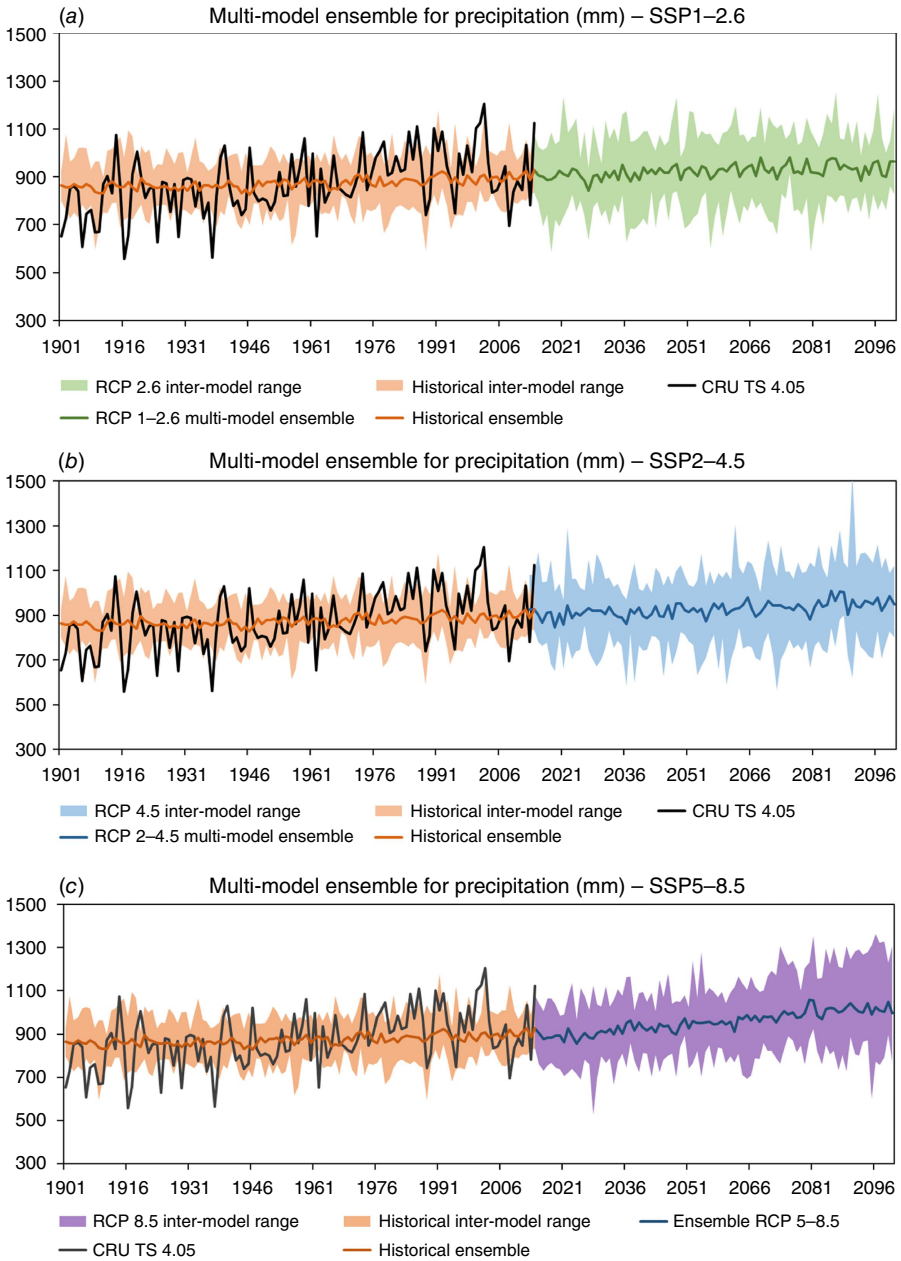

Fig. 8. Observed and bias-corrected model-simulated total annual precipitation in the historical period (1901–2014) and bias-corrected simulated future precipitation (2015–2100). Panels (*a*), (*b*) and (*c*) correspond to scenarios SSP1–2.6, SSP2–4.5 and SSP5–8.5. Historical and future multi-model ensemble simulations were performed using the multi-member mean simulations of 19 analysed GCMs (see Table 1). Shaded areas represent inter-model ranges.

CCR. Although the seasonal cycle is reasonably well represented, considerable inter-model variability persists, especially during the rainy season. This variability represents a key source of uncertainty that should be carefully considered when interpreting future projections.

Future temperature projections indicate a consistent warming trend throughout the 21st Century, with the magnitude of warming strongly dependent on the combination of socioeconomic development and emissions trajectories. Under the fossil-fuelled development and high-emissions SSP5–8.5 scenario, the mean annual temperature is projected to increase by ~3.5°C by 2100. In the middle-of-the-road SSP2–4.5 scenario, this increase is more moderate at 1.3°C, whereas in the sustainable development and low-emissions SSP1–2.6 scenario, the projected rise is only 0.6°C. Notably, the temperature signal intensifies in the latter half of the century, with the greatest warming projected for the northern sector of the CCR.

Projected changes in annual precipitation indicate a slight increase across all scenarios, although with significant uncertainties due to large inter-model ranges and the inherent spatio-temporal variability of precipitation. The projected increase ranges from ~50 mm in the SSP1–2.6 scenario to 80 mm in SSP5–8.5, representing an annual increase of less than 10% relative to the historical mean. Under the SSP5–8.5 scenario, individual model projections range from −20 to +160 mm annually, reflecting substantial spread. This range of uncertainty tends to increase with higher forcing levels, as is

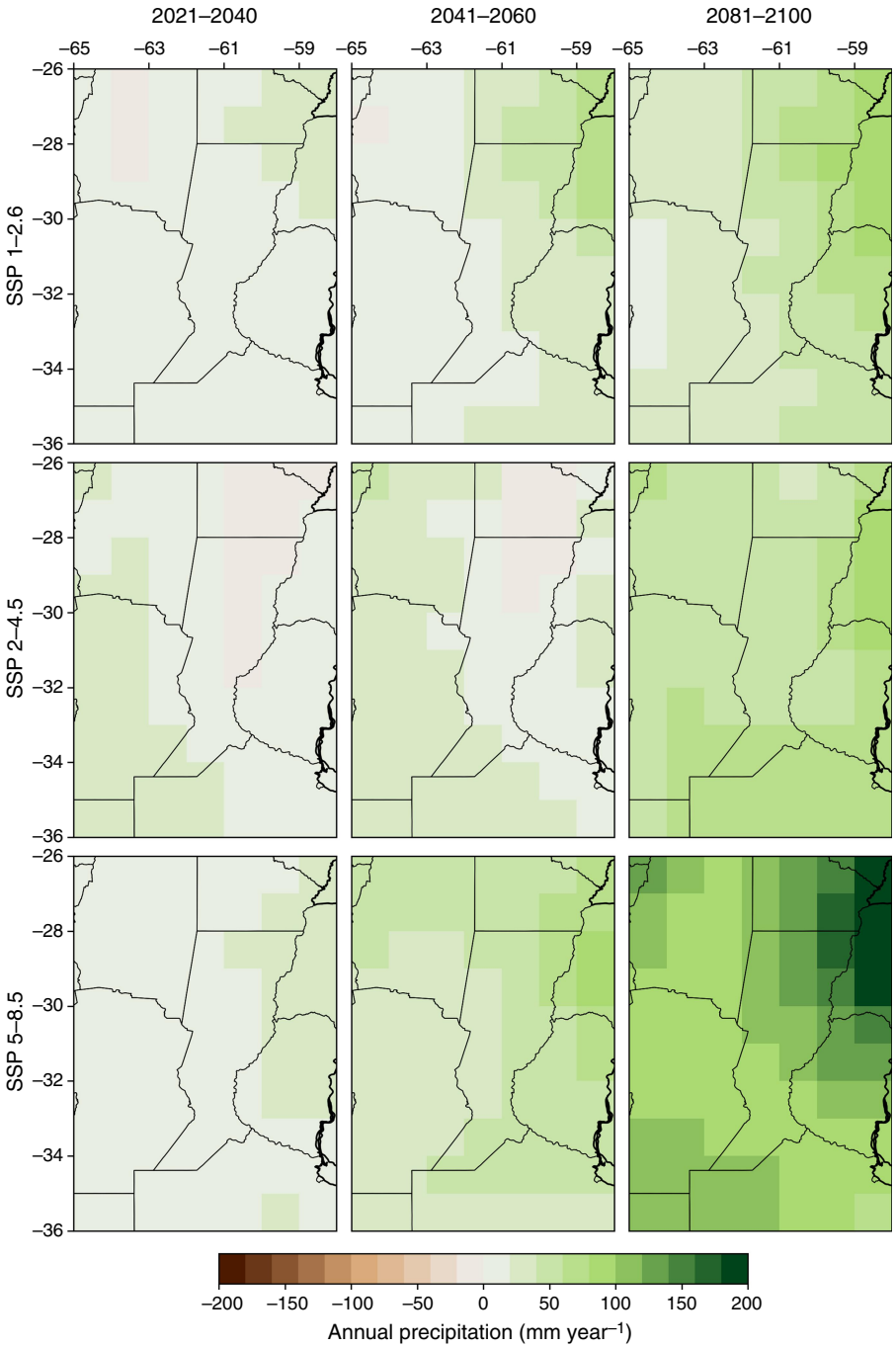

Fig. 9. Spatial distribution of future average changes in total annual precipitation (mm) according to the non-corrected 19-model ensemble over the core crop region in Argentina in the periods (columns) 2021–2040, 2041–2060 and 2081–2100. Average changes are related to the 'near present' 1995–2014 period for the non-corrected 19-model ensemble of the historical simulations. Rows correspond to scenarios SSP1–2.6, SSP2–4.5 and SSP5–8.5.

commonly observed in regional climate projections. Spatially, precipitation increases are more pronounced in the western sector of the CCR, whereas central and eastern areas exhibit lower projected changes. Despite this overall increase, the persistence of historical model biases in underestimating precipitation suggests caution in interpreting these results, particularly regarding their implications for hydrological processes and water availability.

These findings emphasise the need for a nuanced understanding of climate change impacts in one of the world's most agriculturally important regions. Although temperature increases are robust across all scenarios, precipitation projections remain highly uncertain, requiring further research to refine model performance and improve the reliability of future projections. The expected rise in temperature, coupled with potential changes in precipitation patterns, underscores the importance of adaptive strategies in agriculture, water management and regional policy planning. Given the CCR's central role in national and global food production, reported climate shifts may alter crop growth cycles (e.g. Lovino *et al.* 2018*b*)

and reduce yields due to heat stress or water limitations – including the increasing risk of flash droughts (Christian *et al.* 2023; Lovino *et al.* 2025). Proactive measures will be essential to mitigate climate risks and ensure the resilience of agricultural production in the face of ongoing and future climate changes.

References

Allen MR, de Coninck H, Dube OP, *et al.* (2018*a*) Technical summary. In 'Global Warming of 1.5°C. An IPCC Special Report on the impacts of global warming of 1.5°C above pre-industrial levels and related global greenhouse gas emission pathways, in the context of strengthening the global response to the threat of climate change, sustainable development, and efforts to eradicate poverty'. (Eds V Masson-Delmotte, P Zhai, HO Pörtner, D Roberts, *et al.*) pp. 27–46. (Cambridge University Press: Cambridge, UK and New York, NY, USA) doi:10.1017/9781009157940.002

Allen MR, Babiker M, Chen Y, de Coninck H, Connors S, van Diemen R, Dube OP, Ebi KL, Engelbrecht F, Ferrat M, Ford J, Forster P, *et al.* (2018*b*) Summary for policymakers. In 'Global Warming of 1.5°C. An IPCC Special Report on the impacts of global warming of 1.5°C above pre-industrial levels and related global greenhouse gas emission pathways, in the context of strengthening the global response to the threat of climate change, sustainable development, and efforts to eradicate poverty'. (Eds V Masson-Delmotte, P Zhai, HO Pörtner, *et al.*) pp. 3–24. (Cambridge University Press: Cambridge, UK, and New York, NY, USA) doi:10.1017/9781009157940

Almazroui M, Saeed F, Saeed S, *et al.* (2020) Projected change in temperature and precipitation over africa from CMIP6. *Earth Systems and Environment* **4**, 455–475. doi:10.1007/s41748-020-00161-x

Almazroui M, Ashfaq M, Islam MN, *et al.* (2021) Assessment of CMIP6 performance and projected temperature and precipitation changes over South America. *Earth Systems and Environment* **5**, 155–183. doi:10.1007/s41748-021-00233-6

Avila-Diaz A, Torres RR, Zuluaga CF, *et al.* (2023) Current and future climate extremes over Latin America and the Caribbean: assessing Earth system models from high-resolution model Intercomparison project (HighResMIP). *Earth Systems and Environment* **7**, 99–130. doi:10.1007/s41748-022-00337-7

Barros V, Doyle M, Camilloni I (2008) Precipitation trends in southeastern South America: relationship with ENSO phases and low-level circulation. *Theoretical and Applied Climatology* **93**, 19–33. doi:10.1007/s00704-007-0329-x

Barros VR, Boninsegna JA, Camilloni IA, Chidiak M, Magrín GO, Rusticucci M (2014) Climate change in Argentina: trends, projections, impacts and adaptation. *Wiley Interdisciplinary Reviews: Climate Change* **5**(6), 777–797. doi:10.1002/wcc.316

Bigolin T, Talamini E (2024) Impacts of climate change scenarios on the corn and soybean double-cropping system in Brazil. *Climate* **12**(3), 42. doi:10.3390/cli12030042

Brêda JPLF, Dias de Paiva RC, Siqueira VA, Collischonn W (2023) Assessing climate change impact on flood discharge in South America and the influence of its main drivers. *Journal of Hydrology* **624**, 129284. doi:10.1016/j.jhydrol.2023.129284

Carril AF, Cavalcanti IFA, Menéndez CG, *et al.* (2016) Extreme events in the La Plata Basin: a retrospective analysis of what we have learned during CLARIS-LPB project. *Climate Research* **68**, 95–116. doi:10.3354/cr01374

Carvalho D, Cardoso Pereira S, Rocha A (2021) Future surface temperatures over Europe according to CMIP6 climate projections: an analysis with original and bias-corrected data. *Climatic Change* **167**, 10. doi:10.1007/s10584-021-03159-0

Castellanos E, Lemos MF, Astigarraga L, *et al.* (2022) Central and South America. In 'Climate Change 2022: Impacts, Adaptation, and Vulnerability. Contribution of Working Group II to the Sixth Assessment Report of the Intergovernmental Panel on Climate Change'. (Eds H-O Pörtner, DC Roberts, M Tignor, *et al.*) pp. 1689–1816. (Cambridge University Press: Cambridge, UK, and New York, NY, USA) doi:10.1017/9781009325844.014.

Cavalcanti IFA, Carril AF, Penalba OC, *et al.* (2015) Precipitation extremes over La Plata Basin – review and new results from observations and climate simulations. *Journal of Hydrology* **523**, 211–230. doi:10.1016/j.jhydrol.2015.01.028

Christian JI, Martin ER, Basara JB, Furtado JC, Otkin JA, Lowman LE, *et al.* (2023) Global projections of flash drought show increased risk in a warming climate. *Communications Earth & Environment* **4**(1), 165. doi:10.1038/s43247-023-00826-1

Déqué M (2012) Continuous variables. In 'Forecast Verification – A Practitioner's Guide in Atmospheric Science', 2nd edn. (Eds IT Jolliffe, DV Stephenson) pp. 97–120. (Wiley: Chichester, UK)

Deser C (2020) Certain uncertainty: the role of internal climate variability in projections of regional climate change and risk management. *Earth's Future* **8**(12), e2020EF001854. doi:10.1029/2020EF001854

Eyring V, Bony S, Meehl GA, Senior CA, Stevens B, Stouffer RJ, Taylor KE (2016) Overview of the Coupled Model Intercomparison Project Phase 6 (CMIP6) experimental design and organization. *Geoscientific Model Development* **9**, 1937–1958. doi:10.5194/gmd-9-1937-2016

Eyring V, Cox PM, Flato GM, Gleckler PJ, Abramowitz G, Caldwell P, Friedlingstein P (2019) Taking climate model evaluation to the next level. *Nature Climate Change* **9**(2), 102–110. doi:10.1038/s41558-018-0355-y

Feron S, Cordero RR, Damiani A, *et al.* (2019) Observations and projections of heat waves in South America. *Scientific Reports* **9**, 8173. doi:10.1038/s41598-019-44614-4

Formetta G, Feyen L (2019) Empirical evidence of declining global vulnerability to climate-related hazards. *Global Environmental Change* **57**, 101944. doi:10.1016/j.gloenvcha.2019.05.004

Gallardo C, Gil V, Tejeda C, Sánchez E, Gaertner MA (2016) Köppen–Trewartha classification used to assess climate changes simulated by a regional climate model ensemble over South America. *Climate Research* **68**, 137–149. doi:10.3354/cr01340

Garreaud RD, Vuille M, Compagnucci R, Marengo J (2009) Present-day South American climate. *Palaeogeography, Palaeoclimatology, Palaeoecology* **281**(3–4), 180–195. doi:10.1016/j.palaeo.2007.10.032 ISSN 0031-0182

Grimm AM (2019) South American monsoon and its extremes. In 'Remote Sensing of Hydrological Extremes'. (Ed. V Lakshmi) pp. 57–78. (Elsevier) doi:10.1016/B978-0-12-809248-4.00003-0

Hagen I, Huggel C, Ramajo L, Chacón N, Ometto P, Postigo JC, Castellanos EJ (2022) Climate change-related risks and adaptation potential in Central and South America during the 21st Century. *Environmental Research Letters* **17**(3), 033002. doi:10.1088/1748-9326/ac5271

Harris I, Osborn TJ, Jones P, Lister D (2020) Version 4 of the CRU TS monthly high-resolution gridded multivariate climate dataset. *Scientific Data* **7**(1), 109. doi:10.1038/s41597-020-0453-3

Jacob D, Elizalde A, Haensler A, Hagemann S, Kumar P, Podzun R, Rechid D, Remedio AR, Saeed F, Sieck K, Teichmann C, Wilhelm C (2012) Assessing the transferability of the regional climate model REMO to different coordinated regional Climate Downscaling Experiment (CORDEX) regions. *Atmosphere* **3**(1), 181–199. doi:10.3390/atmos3010181

Junquas C, Vera C, Li L, *et al.* (2012) Summer precipitation variability over southeastern South America in a global warming scenario. *Climate Dynamics* **38**, 1867–1883. doi:10.1007/s00382-011-1141-y

Kim Y, Min SK, Son SW, Kwon WT (2020) Evaluation of CMIP6 multi-model ensemble for temperature and precipitation over East Asia. *Climate Dynamics* **54**(3–4), 3237–3260. doi:10.1007/s00382-020-05298-3

Lee J-Y, J Marotzke, G Bala, L Cao, S Corti, JP Dunne, F Engelbrecht, E Fischer, JC Fyfe, C Jones, A Maycock, J Mutemi, O Ndiaye, S Panickal, T Zhou (2021) Future global climate: scenario-based projections and near-term information. In 'Climate Change 2021: The Physical Science Basis. Contribution of Working Group I to the Sixth Assessment Report of the Intergovernmental Panel on Climate Change'. (Eds V Masson-Delmotte, P Zhai, A Pirani, SL Connors, C Péan, S Berger, N Caud, Y Chen, L Goldfarb, MI Gomis, M Huang, K Leitzell, E Lonnoy, JBR Matthews, TK Maycock, T Waterfield, O Yelekçi, R Yu, B Zhou) pp. 553–672. (Cambridge University Press: Cambridge, UK, and New York, NY, USA) doi:10.1017/9781009157896.006

Lehner F, Deser C, Maher N, Marotzke J, Fischer EM, Brunner L, *et al.* (2020) Partitioning climate projection uncertainty with multiple large ensembles and CMIP5/6. *Earth System Dynamics* **11**(2), 491–508. doi:10.5194/esd-11-491-2020

Lovino MA, Müller OV, Berbery EH, Müller GV (2018*a*) How have daily climate extremes changed in the recent past over northeastern

Argentina? *Global and Planetary Change* **168**, 78–97. doi:10.1016/j.gloplacha.2018.06.008

Lovino MA, Müller OV, Berbery EH, Müller GV (2018*b*) Interannual-to-multidecadal hydroclimate variability and its sectoral impacts in northeastern Argentina. *Hydrology and Earth System Sciences* **22**, 3155–3174. doi:10.5194/hess-22-3155-2018

Lovino MA, Pierrestegui MJ, Müller OV, Berbery EH, Müller GV, Pasten M (2021) Evaluation of historical CMIP6 model simulations and future projections of temperature and precipitation in Paraguay. *Climatic Change* **164**, 46. doi:10.1007/s10584-021-03012-4

Lovino MA, Pierrestegui MJ, Masaro L, Müller OV, Müller GV, Berbery EH (2025) Agricultural flash droughts and their impact on crop yields in southeastern South America. *Environmental Research Letters* **20**(5), 054058. doi:10.1088/1748-9326/adcd88

Maraun D, Wetterhall F, Ireson AM (2010) Precipitation downscaling under climate change: recent developments to bridge the gap between dynamical models and the end user. *Reviews of Geophysics* **48**, RG3003. doi:10.1029/2009RG000314

Masson-Delmotte V, Zhai P, Pirani A, Connors SL, Péan C, Berger S, Caud N, Chen Y, Goldfarb L, Gomis MI, Huang M, K Leitzell, Lonnoy E, Matthews JBR, Maycock TK, Waterfield T, Yelekçi O, Yu R, Zhou B (Eds) (2021) 'Climate Change 2021: The Physical Science Basis. Contribution of Working Group I to the Sixth Assessment Report of the Intergovernmental Panel on Climate Change.' (Cambridge University Press: Cambridge, UK, and New York, NY, USA) doi:10.1017/9781009157896

Ministerio de Agricultura, Ganadería y Pesca de Argentina (2021) Resultados Agrícolas (Ingresos – Gastos – Márgenes): Campaña Agrícola 2021/2022 Septiembre 2021. (MAGyP) Available at https://www.magyp.gob.ar/sitio/areas/analisis_economico/margenes/_archivos//000001_Informes%20de%20M%C3%A1rgenes%20y%20Resultados/202100_2021/210900_Margenes%20Resultados%20(Septiembre%202021).pdf [In Spanish]

Moriasi DN, Arnold JG, Van Liew MW, Bingner RL, Harmel RD, Veith TL (2007) Model evaluation guidelines for systematic quantification of accuracy in watershed simulations. *Transactions of the ASABE* **50**(3), 885–900. doi:10.13031/2013.23153

Müller GV, Lovino MA, Sgroi LC (2021) Observed and projected changes in temperature and precipitation in the core crop region of the Humid Pampa, Argentina. *Climate* **9**(3), 40. doi:10.3390/cli9030040

Muluneh MG (2021) Impact of climate change on biodiversity and food security: a global perspective – a review article. *Agriculture & Food Security* **10**, 36. doi:10.1186/s40066-021-00318-5

Nash JE, Sutcliffe JV (1970) River flow forecasting through conceptual models part I – a discussion of principles. *Journal of Hydrology* **10**(3), 282–290. doi:10.1016/0022-1694(70)90255-6

Oñate-Valdivieso F, Uchuari V, Oñate-Paladines A (2020) Large-scale climate variability patterns and drought: a case of study in South America. *Water Resources Management* **34**, 2061–2079. doi:10.1007/s11269-020-02549-w

O'Neill B (2016) The Shared Socioeconomic Pathways (SSPs) and their extension and use in impact, adaptation and vulnerability studies. (Purdue University, Center for Global Trade Analysis, Global Trade Analysis Project) Available at https://ageconsearch.umn.edu/record/332808/files/8175.pdf

O'Neill BC, Tebaldi C, van Vuuren DP (2016) The scenario model intercomparison project (ScenarioMIP) for CMIP6. *Geoscientific Model Development* **9**, 3461–3482. doi:10.5194/gmd-9-3461-2016

Riahi K, van Vuuren DP, Kriegler E, Edmonds J, O'Neill BC, Fujimori S, Bauer N, Calvin K, Dellink R, Fricko O, Lutz W, Popp A, Cuaresma JC, KC S, Leimbach M, Jiang L, Kram T, Rao S, Emmerling J, Ebi K, Hasegawa T, Havlik P, Humpenöder F, Da Silva LA, Smith S, Stehfest E, Bosetti V, Eom J, Gernaat D, Masui T, Rogelj J, Strefler J, Drouet L, Krey V, Luderer G, Harmsen M, Takahashi K, Baumstark L, Doelman JC, Kainuma M, Klimont Z, Marangoni G, Lotze-Campen H, Obersteiner M, Tabeau An, Tavoni M (2017) The shared socioeconomic pathways and their energy, land use, and greenhouse gas emissions implications: an overview. *Global Environmental Change* **42**, 153–168. doi:10.1016/j.gloenvcha.2016.05.009

Seager R, Naik N, Baethgen W, Robertson A, Kushnir Y, Nakamura J, Jurburg S (2010) Tropical oceanic causes of interannual to multidecadal precipitation variability in southeast South America over the past century. *Journal of Climate* **23**, 5517–5539. doi:10.1175/2010JCLI3578.1

Sgroi LC, Lovino MA, Berbery EH, Müller GV (2021) Characteristics of droughts in Argentina's core crop region. *Hydrology and Earth System Sciences* **25**(5), 2475–2494. doi:10.5194/hess-25-2475-2021

Skansi MM, Brunet M, Sigró J, Aguilar E, Arevalo Groening JA, Bentancur OJ, Castellón Geier YR, Correa Amaya RL, Jácome H, Malheiros Ramos A, Oria Rojas C, Pasten AM, Sallons Mitro S, Villaroel Jiménez C, Martínez R, Alexander LV, Jones PD (2013) Warming and wetting signals emerging from analysis of changes in climate extreme indices over South America. *Global and Planetary Change* **100**, 295–307. doi:10.1016/j.gloplacha.2012.11.004

Tebaldi C, Debeire K, Eyring V, Fischer E, Fyfe J, Friedlingstein P, Knutti R, Lowe J, O'Neill B, Sanderson B, van Vuuren D, Riahi K, Meinshausen M, Nicholls Z, Tokarska KB, Hurtt G, Kriegler E, Lamarque J-F, Meehl G, *et al.* (2021) Climate model projections from the Scenario Model Intercomparison Project (ScenarioMIP) of CMIP6. *Earth System Dynamics* **12**(1), 253–293. doi:10.5194/esd-12-253-2021

Tian J, Zhang Z, Ahmed Z, *et al.* (2021) Projections of precipitation over China based on CMIP6 models. *Stochastic Environmental Research and Risk Assessment* **35**, 831–848. doi:10.1007/s00477-020-01948-0

World Bank (2024) Argentina: towards a more competitive, inclusive, and resilient agri-food sector. (The World Bank: Washington, DC, USA) Available at https://documents1.worldbank.org/curated/en/099042825141510674/pdf/P179104-ced545dd-f942-4770-a032-089037e12d2a.pdf

Zambrano F, Vrieling A, Nelson A, Meroni M, Tadesse T (2018) Prediction of drought-induced reduction of agricultural productivity in Chile from MODIS, rainfall estimates, and climate oscillation indices. *Remote Sensing of Environment* **219**, 15–30. doi:10.1016/j.rse.2018.10.006

Zareian M, Dehban H, Gohari A (2024) Assessment of CMIP6 models performance in simulation precipitation and temperature over Iran and surrounding regions. *Environmental Monitoring and Assessment* **196**, 701. doi:10.1007/s10661-024-12878-7

Zazulie N, Rusticucci MM, Raga GB (2017) Regional climate of the subtropical central Andes using high-resolution CMIP5 models – part I: past performance (1980–2005). *Climate Dynamics* **49**(11–12), 3937–3957. doi:10.1007/s00382-017-3560-x

Zhang L, Yu X, Zhou T (2023) Understanding and attribution of extreme heat and drought events in 2022: current situation and future challenges. *Advances in Atmospheric Sciences* **40**, 1941–1951. doi:10.1007/s00376-023-3171-x

Data availability. The CRU TS version 4.05 dataset (Harris *et al.* 2020), developed by the Climatic Research Unit at the University of East Anglia, can be accessed at https://catalogue.ceda.ac.uk/uuid/c26a65020a5e4b80b20018f148556681/. The CMIP6 multi-model outputs (Eyring *et al.* 2016) are publicly available through the Earth System Grid Federation portal at https://esgf-node.ipsl.upmc.fr/search/cmip6-ipsl/.

Conflicts of interest. The authors declare that they have no conflicts of interest

Declaration of funding. This work was funded by the Consejo Nacional de Investigaciones Cientificas y Técnicas (CONICET) from Argentina, PIP-CONICET project 11220200102257CO.

Author affiliations
[A]Consejo Nacional de Investigaciones Científicas y Técnicas (CONICET), Santa Fe, Argentina.
[B]Centro de Variabilidad y Cambio Climático (CEVARCAM), Facultad de Ingeniería y Ciencias Hídricas (FICH), Universidad Nacional del Litoral (UNL), Ciudad Universitaria, Santa Fe, Argentina.